Control features of the electromechanical system with end-effector considering the regulated torque

Andrei Malchikov*, *Andrei* Yatsun, *Petr* Bezmen and *Oleg* Tarasov
Southwest State University, Department of Mechanics, Mechatronics and Robotics, 305040 Kursk, Russia

Abstract. The article describes the features of digital control of an electromechanical system consisting of an electric drive, a load and a feedback system. The emphasis is on implementing a mode in which the electric drive torque can be adjusted. These results can be applied in service and industrial robotics.

1. Introduction

Effective functioning of the most of robotic systems is possible only under the following conditions: the controlled consumption of the power source, the optimal motion laws and controlled force-moment parameters of the mechanism actuating links.

High energetic efficiency of a robot is achieved by using modern productive electric drives with mechanical transmissions with a high coefficient of efficiency and optimal circuit solutions [1, 2]. One of the modern approaches to provide the efficiency of the drive is monitoring power consumption and heat losses during the execution of the required motion laws. This aim can be achieved by using a double loop control system, in which torque and motor current control are implemented in addition to end-effector position control. This method is especially relevant for mobile systems, in which the cruising range of the robot is determined by the limited battery capacity.

The example of such a system is an assistive powered exoskeleton (Fig. 1) that enables a person with lower-limb disabilities to perform upright gait, climb stairs and perform simple body movements [3-8]. It is also important for exoskeleton system to ensure torque limitation to guarantee smooth motion of the drives, user safety and long life of the mechanical transmissions.

This paper compares two approaches to design a control system the end-effector position of the electromechanical system. The first approach is based on a classic control system for the rotation angle of the end-effector without the motor torque and winding current feedback. The second one is the implementation of a double loop control system that takes into account the real-time data of the current sensors and provides the required torque limitation.

Fig. 1. Assistive powered exoskeleton ExoLite.

The authors present both the results of a numerical experiment on the mathematical model of the mechatronic drive, and the results of full-scale tests on a laboratory bench. A comparative analysis of the obtained results is made and conclusions are drawn.

2. Analytical model of the system

Figure 2 shows the analytical model of the experimental electromechanical system consisting of a mass 1 fixed to the link 2. The link 2 is driven by an electric drive consisting of a DC-motor 4 and a reducer 3.

The device works in the following way. A control signal with the desired angle φ* and current *I** values and real-time data from the feedback sensor 8 (*I*' value) and the feedback sensor 9 (φ' value) comes in the inputs of the control system 6, consisting of a controller unit and the comparator unit.

The controller unit generates an output signal *u**, which is fed to the power amplifier 7 and after the control voltage *u* goes to the DC-motor 4.

* Corresponding author: teormeh@inbox.ru

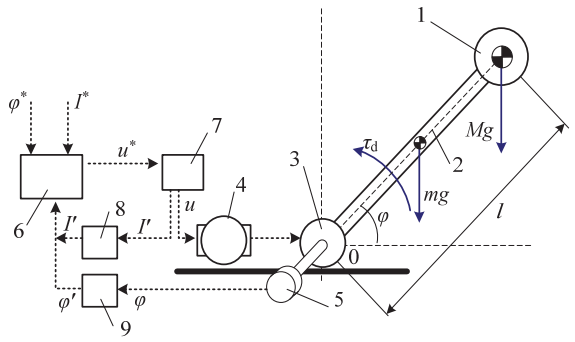

Fig. 2. The analytical model of the experimental electromechanical system.

3. Mathematical model of the mechatronical system

During investigation of the system mathematical model the following assumptions were made: the links of the system are absolutely rigid, the gaps are neglected in the reducer 3, the saturation of the magnetic flux in the motor simulation is not considered, dry friction forces act according to the Coulomb model and the viscous component is represented by a linear model. Then the equations describing the processes taking place in the mechatronic system can be written in the form:

$$\begin{cases} J\ddot{\varphi} = \tau_d - \tau_\mu - \tau_b - Mgl\cos\varphi - \dfrac{mgl\cos\varphi}{2} \\ L\dfrac{dI}{dt} + RI + c_E(\dot{\varphi}\cdot i_r) = u \end{cases}, \quad (1)$$

In this case, the torques acting on the system are described by the following equations:

- the electric drive torque is equal to:

$$\tau_d = c_M I \cdot i_r \eta, \quad (2)$$

- the viscous resistance moment is equal to:

$$\tau_b = \beta\dot{\varphi}, \quad (3)$$

- the dry friction force moment equation is equal to:

$$\tau_\mu = \begin{cases} -\tau_\mu^* \operatorname{sign}(\dot{\varphi}), \ \text{if} \ \dot{\varphi} \neq 0; \\ -\sum_{j=0}^{n}\tau_j, \ \text{if} \ \dot{\varphi} = 0 \ \text{and} \ \left|\sum_{j=0}^{n}\tau_j\right| \le \tau_\mu^*; \\ -\tau_\mu^* \operatorname{sign}\left(\sum_{j=0}^{n}\tau_j\right), \ \text{if} \ \dot{\varphi} = 0 \ \left|\sum_{j=0}^{n}\tau_j\right| > \tau_\mu^*. \end{cases} \quad (4)$$

The following denotations are used in above-mentioned formulas: M – the mass of the body fixed on the link, m – the link mass, l – the length of the link, J – the inertia equivalent moment of the system:

$$J = \frac{ml^2}{3} + Ml^2 \quad (5)$$

I – the motor winding current; R – the motor winding active resistance; i_r - the total reduction ratio of the reducer; η - the efficiency coefficient of mechanical transmission; c_M - the motor moment coefficient; c_E - the motor anti-electromotive force coefficient; β - the viscous resistance coefficient; τ_μ^* - the dry friction limiting moment, τ_j - the sum of all external force moments, excluding moments of frictional forces.

4. Control system description

In the simplest case, the drive must be equipped with a closed-loop control system to ensure the required position of the link. The functional diagram of the closed-loop control system is shown in Figure 3.

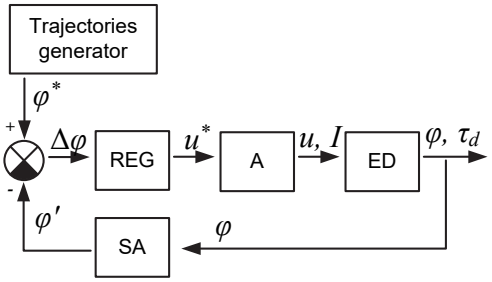

Fig. 3. Block diagram of the closed-loop control system.

The following denotations are used in Figure 3: REG. – the regulator, A – the power amplifier, ED – the electric drive, SA – the angle sensor.

In this case, the power supplied to the drive (u, I) is determined by the error ($\Delta\varphi$) value – the difference between the measured angle (φ') of the actuator and the required angle (φ^*).

In this case, P-, PI- or PID- controllers and other types of controllers, such as fuzzy logic controllers can be used.

In this paper we consider a PD-controller, for which the u^* signal value is defined as:

$$u^* = k_p e + k_d \dot{e}, \quad (6)$$

where k_p, k_d – the controller amplification coefficients.

$$e = \varphi^* - \varphi' \quad (7)$$

$$\dot{e} = \dot{\varphi}^* - \dot{\varphi}' \quad (8)$$

In mechatronic systems, P-regulators and PID-controllers are widely used to create a position control system [2-5], but in practice PD- controllers are also used, which are much easier to configure using, among other methods, manual tuning methods [10, 11]. We note that the evaluation of the integral component in

the PID controller requires significant computational power of the control system [10].

With this control approach the motor current can be determined by the load on the final link. Thus, in the event of jamming or other unforeseen situations, the engine may fail or the mechanical transmission can be damaged. Usually modern controllers have adjustable protection against overheating or current limits. However, the values of these current limits cannot be changed during the movement of the device, which is especially important for multi-link systems, in which the load moment on the reducer can be determined by the system configuration and cannot be predetermined. To ensure the protection of the mechanical part of the drive, torque monitoring and the possibility to adjust the limits depending on the configuration of the mechanism are required. This is possible only when current data is taken into account directly by the control system in real-time mode.

To ensure the protective properties of the system and to provide the required parameters of energy efficiency, the authors propose a double loop control system (Fig. 4).

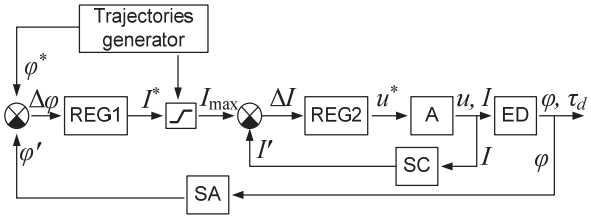

Fig. 4. Block diagram of the double loop control system.

Some denotations in Figure 4 are similar to those in Figure 3. In this case the power supplied to the drive (u, I) is not only determined by the angle error ($\Delta\varphi$), but also determined by the current error value (ΔI) obtained by comparing the current generated by the local feedback and the current value received from the sensor, denoted on the diagram as C.

Thus, the operation of the controller is described by the equation of the control signal at the amplifier input:

$$u^* = k_p^I e^I, \tag{9}$$

where k_p^I – the proportional coefficient of the current regulator (REG2 – see Fig. 4). The mistake is defined as:

$$e^I = I^* - I' \tag{10}$$

The required current value is limited by the current value $I_{\max}$ obtained from the control action generator.

$$I^* = \begin{cases} I_{\max} \ if \ \left(I^* \geq I_{\max}\right) \\ I^* \ if \ \left(I^* < I_{\max}\right) \end{cases} \tag{11}$$

The initial value I^* is determined by the loop of the angle control, as follows:

$$I^* = k_p^\varphi e^\varphi + k_d^\varphi \dot{e}^\varphi \tag{12}$$

where k_p, k_d – the gain coefficients of the position controller (REG1 – see Fig. 3);

$$e^\varphi = \varphi^* - \varphi' \tag{13}$$

$$\dot{e}^\varphi = \dot{\varphi}^* - \dot{\varphi}^* \tag{14}$$

5. Results of mathematical modelling

Further we study the end-point control features. To do that we numerically integrate the system of equations (1) describing the motion of the link (the actuating link). In this case, the electric drive torque value is determined by the equation (2), and the moments of friction and viscous resistance forces by equations (3) and (4). To simulate an angular position control system, we use equations (5) and for a system with current limitation – equations (8), (10), and (11). A program was developed for numerical calculation in the MathCad software to obtain the solution.

The primary objective of modeling is to study system's operation features in the presence of a motor current limit and the result of controlling the torque on the actuating link. We obtain graphs of the system behavior for different values $I_{\max}$ for the following types of control signals (Fig. 5):

- stepped signal,
- rectangular signal.

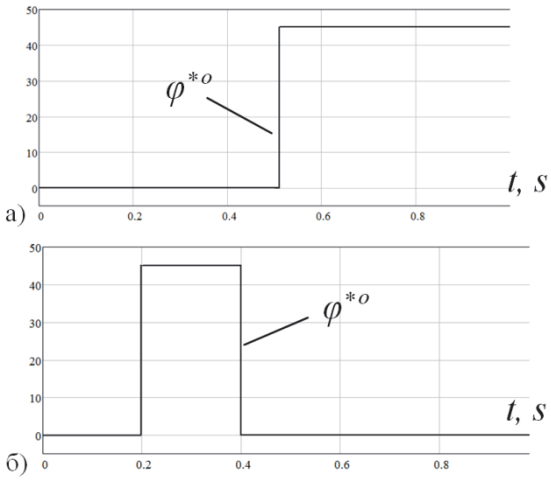

Fig. 5. Types of control signal used for simulation: a – stepped signal, b – rectangular signal.

The electromechanical system parameters used in the simulation were taken in accordance with the parameters of the experimental bench, which was created for debugging the mathematical model and conducting full-scale tests on the control system (Table 1).

We consider the modeling results for stepped control signal with an amplitude of 45 degrees (Fig. 6), and a tuned angular position control system (coefficients $k_p = 3.4$, $k_d = 4$).

Table 1. The mathematical model parameters.

Parameter name	Value
The link mass, *m*	0.005 kg
The mass of the body fixed on the link, *M*	0.024 kg
The length of the link, *l*	0.11 m
Operating supply voltage, U_{nom}	12 V
The motor armature active resistance, R	2.4 Ohm
The motor moment coefficient, C_M	0.0055
The motor anti-electromotive force coefficient, CE	0.0055
The total reduction ratio of the reducer, ir	30
The efficiency coefficient of mechanical transmission, η	0.85
The accuracy of the sensor, taking into account the reducer	0.4°
The sampling rate of the feedback sensor	500 Hz
The dry friction limiting moment, τ_{μ}^{*}	0.01 Nm
The viscous resistance coefficient, β	0.0001 Nm·s

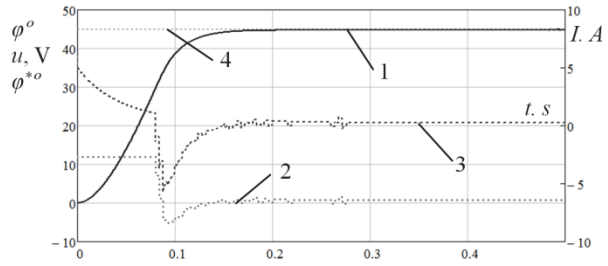

Fig. 6. Results of the angular position control system modeling at stepped control signal: 1 – angular position of the link, φ; 2 – control voltage, u; 3 – current, I; 4 – required angular position φ* of the link (stepped control signal).

We can see that the current value is 5 A at the electric motor start-up and reaches 6 A when the voltage is reversed.

Further, we show an example that demonstrates the results of rectangular control signal influence. In this case, the signal changes instantaneously by a significant amount (Fig. 5, b). Figure 7 shows that the required angular position changes from 60° to 0° at 0.06 sec.

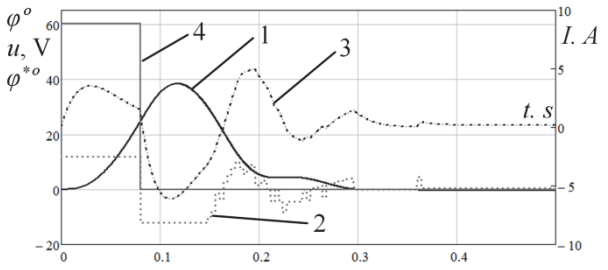

Fig. 7. Results of the angular position control system modeling at rectangular control signal: 1 – angular position of the link, φ; 2 – control voltage, *u*; 3 – current, *I*; 4 – required angular position φ^{*} of the link (rectangular control signal).

Figure 8 shows the character of the variation of the link angular position and the motor current when current feedback is used without limitations.

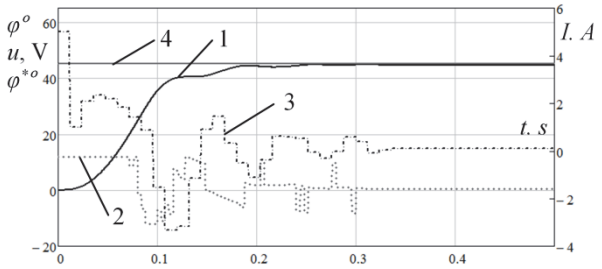

Fig. 8. Results of the control system modeling with using of current limitation: 1 – angular position of the link, φ; 2 – control voltage, *u*; 3 – current, *I*; 4 – required angular position φ^{*} of the link (stepped control signal).

In this case, the motor current can reach 7 A, which can lead to damage of the motor insulation or the mechanical transmission elements. A similar situation can also arise when an external force appears, which can result in significant current and forces in the reducer.

The control system of the link position with the torque control makes it possible to reduce the motor current in the transient processes while providing the required operating mode of the electric drive.

Addition of the current control loop increased the transient time to 0.3 sec as compared to single-loop control system (Fig. 9). An oscillatory character of the link's motion also occurred due to an overshoot in the feedback loop.

Further, we consider the modeling results for a stepped control signal and different values of the limiting current.

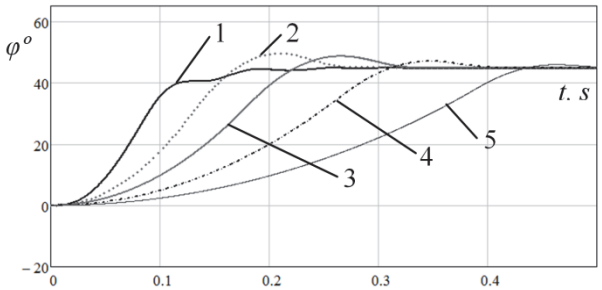

Fig. 9. Control system simulation results for a stepped control signal with current limitation: 1 - limitation 5A, 2 - limitation 1.5A, 3 - limitation 1A, 4 - limitation 0.7A, 5 - limitation 0.55A.

We can see from the numerical simulation results that limiting the maximum current preserves the system's operability but changes the parameters of the transient process. When a current limitation of 0.55 A is introduced under stepped control signal the transient time can be more than 0.5 sec and the overshoot value also changes. The current limitation does not allow the system to stop instantly – a motor rundown can be seen in the graphs. To ensure the required parameters of the transient process it is necessary to set the controller coefficients for each limiting value separately.

The simulation results for a rectangular control signal and different values of the limiting current are shown in Figure 10.

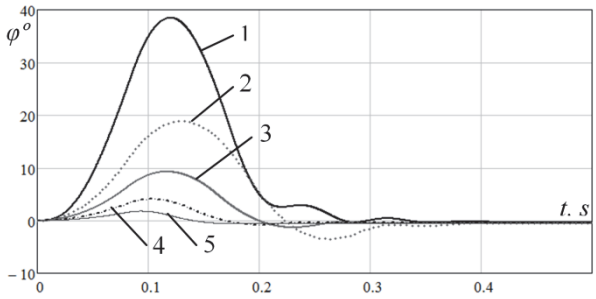

Fig. 10. Control system simulation results at the rectangular control signal with current limitation: 1 - limitation 5A, 2 - limitation 1.5A, 3 - limitation 1A, 4 - limitation 0.7A, 5 - limitation 0.55A

Modeling the system under a rectangular control signal (the pulse duration is 0.1 sec) made it possible to establish that the transient process time is 0.4 sec without current limitation. The transient process takes approximately the same time with current limitations of 0.7 and 0.5 A. However, the link does not execute the required amplitude of motion when the motor current is limited and overshoot and oscillation can also arise.

Conclusion

As shown by the simulation results motor current limitation makes it possible to avoid exceeding the torque during acceleration and braking of the motor, which then reduces the load on the electric motor and reducer of the electric drive.

However, the introduction of the input power limitation significantly changes the nature of the actuating link's movement. Current limitation increases the duration of the transient process, while an instantaneous change of the control action allows system rundown, which can lead to undesired overshoot of the control system. In order to guarantee the required system parameters, additional tuning for a specific value of the maximum current is required.

Supported from grant of the President of the Russian Federation for young scientists MK-2701.2017.8

References

1. S. Jatsun, S. Savin, B. Lushnikov, A. Yatsun, *ITM Web of Conferences*, **6** (2016).
2. S. Jatsun, S. Savin, A. Yatsun, A. Malchikov, *Advances in intelligent systems and computing,* 371, 165-172 (2015)
3. S.F. Jatsun, L. Yu. Vorochaeva, A.S.Yatsun, S.I. Savin, *International Conference on CLAWAR*, 175-182 (2015)
4. S.F. Jatsun, S.I. Savin, A.S. Yatsun, R.N. Turlapov, *26th DAAAM Intern. Symp. on Intelligent Manufacturing and Automation,* 107-112 (2015)
5. S. Jatsun, A. Malchikov, A. Yatsun, *22nd International Conference on Vibroengineering,* 8 (2016)
6. S.F. Jatsun, P.A. Bezmen, A.S. Yatsun, *22nd International Conference on Vibroengineering,* 8, 403-408 (2016)
7. S.F. Jatsun, S.I. Savin, P.A. Bezmen, *International Conference on Pure Mathematics,* 146-149 (2015)
8. S.F. Jatsun, S.I. Savin, P.A. Bezmen, *International Conference on Pure Mathematics,* 83-87 (2015)
9. L.Yu. Vorochaeva, A.S. Yatsun, S.F. Jatsun, SPIIRAS Proceedings, **3**(52), 70-94 (2017)
10. R. Izerman, *Digital Control Systems* (1984)
11. V.V. Denisenko, Sensors and systems, **6,** 35-38 (2009)
12. K.J. Astrom, T. Hagglund, *The Instrumentation, Systems, and Automation Society* (2006)
13. M. Hassan, H. Kadone, K. Suzuki, Y. Sankai, Sensors. **14**(1) (2016)
14. K. Kiguchi, T. Takakazu, F. Toshio, Fuzzy Systems: IEEE Transactions, **12** (4) (2004)
15. N. Aphiratsakun, P. Manukid, International Journal of Advanced Robotics Systems, **6**(4) (2009)
16. R. Steger, S. Kim, H. Kazerooni, *IEEE International Conference on Robotics and Automation* (2006)
17. J. Pratt, B. Krupp, C. Morse, Industrial Robot: an International Journal, **29**(3) (2002)
18. J.F. Veneman, R. Ekkelenkamp, R. Kruidhof, F.C. van der Helm, H. van der Kooij, The International Journal of Robotics Research, **25**(3) (2006)